

Fig. 3 shows a contour plot of the measured η for the same parameter values used in the calculations. The region of measured conversion efficiencies is limited by the tuning range of the ECL and by the gain bandwidth of the booster amplifier. Comparing Fig. 3 and Fig. 2 good agreement is shown between theory and experiment. Transparent ($\eta > 0$ dB) WC is possible for a maximum signal to pump wavelength detuning of 30.5 nm, corresponding to a WC bandwidth of 61 nm assuming symmetrical up- and down-conversion.

In Fig. 3, level curves representing $\eta > 0$ dB are not included, to better illustrate the vast transparent region. In Fig. 4, η against pump wavelength is plotted to show the pump tuning range. We measured a pump tuning range of 24 nm for transparent WC at $\lambda_S = 1550$ nm. The tunability of 24 nm is in the same range as for SOA wavelength converters [4, 5]. Fig. 4 also shows the good agreement between experiment and theory for $\eta > 0$ dB. The gain ripple is < 5 dB over the transparent pump tuning range.

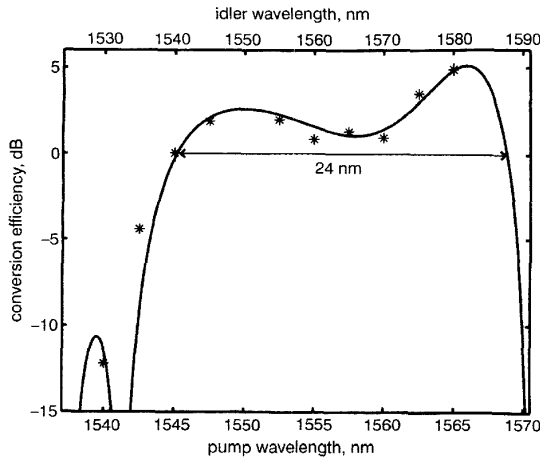


Fig. 4 Measured η against pump and idler wavelength

* idler wavelength
— theory

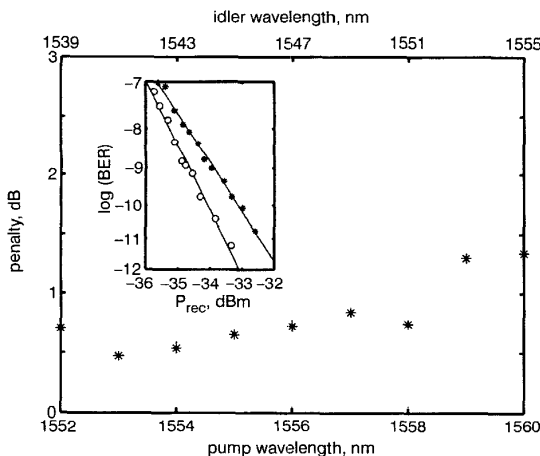


Fig. 5 Power penalty against pump and idler wavelength at $\lambda_S = 1565$ nm

Inset: Back-to-back BER and BER for $\lambda_p = 1556$ nm

○ back-to-back
* $\lambda_p = 1556$ nm

Finally, the quality of the wavelength converter is estimated by measuring bit error rate (BER) and power penalty at $\text{BER} = 10^{-9}$. The signal is externally modulated using a LiNbO_3 Mach-Zehnder (MZ) interferometer with 10 Gbit/s NRZ, $2^{31} - 1$ pseudorandom bit stream (PRBS) data. The pump is filtered by a 4 nm BPF after the booster erbium-doped fibre amplifier (EDFA) before it is combined with the data signal. After WC the idler is filtered out by two 1 nm BPFs, detected by a preamplified receiver and sent to the BER test set. Fig. 5 shows the wavelength conversion power penalty for $\text{BER} = 10^{-9}$ against pump wavelength, for $\lambda_S = 1565$ nm. The back-to-back sensi-

tivity of $\text{BER} = 10^{-9}$ without WC is -34.7 dBm. The penalty is < 1.4 dB, where the penalty increases close to the pump wavelength. This could be explained by the limited noise suppression in the 1 nm filters. The inset in Fig. 5 shows the back-to-back BER and the BER of the converted signal in the case $\lambda_p = 1556$ nm.

Conclusion: We have demonstrated a CW-pumped fibre wavelength converter with a conversion efficiency > 0 dB over a 61 nm conversion bandwidth. We have also demonstrated a pump wavelength tuning range of 24 nm, alleviating one classical SOA wavelength converter advantage. Good conversion quality is verified by BER measurements at 10 Gbit/s, yielding < 1.4 dB power penalty.

© IEE 2002

Electronics Letters Online No: 20020049

DOI: 10.1049/el:20020049

M. Westlund, J. Hansryd and P.A. Andrekson (Chalmers University of Technology, Photonics Laboratory, SE-412 96 Göteborg, Sweden)

E-mail: westlund@elm.chalmers.se

J. Hansryd and P.A. Andrekson: also with CENiX Inc., 6575 Snowdrift Road, Suite 105, Allentown, PA 18106, USA

S.N. Knudsen (Lucent Technologies Denmark, Priorparken 680, DK-2605 Broendby, Denmark)

References

- HANSRYD, J., DROSS, F., WESTLUND, M., ANDREKSON, P.A., and KNUDSEN, S.N.: 'Increase of the SBS threshold in a short highly nonlinear fiber by applying a temperature distribution', *J. Lightwave Technol.*, 2001 (accepted for publication)
- AGRAWAL, P.: 'Nonlinear fiber optics' (Academic Press, 1995), p. 408
- INOUE, K.: 'Four-wave mixing in an optical fiber in the zero-dispersion wavelength region', *J. Lightwave Technol.*, 1992, 10, (11), pp. 1553-1561
- FURUKAWA, H., YOSHIDAYA, H., TAKAKURA, H., and KURODA, K.: 'A novel optical device with wide bandwidth wavelength-conversion, and an optical sampling experiment using this device'. Instrumentation and Measurement Tech. Conf., 1999, Vol. 2, pp. 1143-1148
- HUNZIKER, G., PAIELLA, R., D'OTTAVI, A., SPANO, P., DALL'ARA, R., GUEKOS, G., and VAHALA, G.: '30 nm wavelength conversion at 10 Gbit/s by four-wave mixing in a semiconductor optical amplifier'. OFC '98, Tech Digest, 1998, pp. 108-109

Ultra-sensitive autocorrelation of 1.5 μm light with single photon counting silicon avalanche photodiode

C. Xu, J.M. Roth, W.H. Knox and K. Bergman

1.5 μm two-photon absorption in a single photon counting silicon avalanche photodiode at record continuous-wave levels below 100 μW is reported. Autocorrelation of a 10 GHz, 1.67 picosecond pulsetrain using this device demonstrates 1.5×10^{-3} (mW)² peak-power times average-power sensitivity without the use of lock-in detection.

Introduction: Picosecond and femtosecond pulsewidth measurements contain critical diagnostic information in many fields of optics. Experimentalists have relied most widely on nonlinear autocorrelation techniques for pulsewidth measurements because of their inexpensive and well-studied nature. The nonlinear process enables one to distinguish the pulse from coherent noise, and it most commonly entails second-harmonic generation (SHG) in a crystal followed by electrical detection of the upconverted light. Recently two-photon absorption (TPA) autocorrelations have attracted considerable attention since they achieve a quadratic nonlinearity using simple direct electrical detection in a semiconductor material [1-3]. Furthermore, semiconductor TPA techniques eliminate the need for expensive nonlinear crystals and their associated critical phase-matching alignment with strong polarisation sensitivity. However, the exact functional behaviour of TPA depends upon peak power, and it degrades with higher repetition rates for a given average power. The remedy for this situation typically involves boosting the power in an optical amplifier to perform the

measurement, even though this adds drawbacks such as higher cost, degraded signal-to-noise ratio, and pulsewidth distortion.

Results and discussion: In this Letter we report a novel TPA autocorrelation technique that uses a single photon counting silicon avalanche photodiode (SPAD) to achieve enhanced sensitivity over other TPA techniques. It is important to note that our technique differs uniquely from that reported in [3] since unlike conventional APDs this SPAD device (EG&G, SPCM-AQ-16) is reverse biased above the breakdown voltage, and thus operates like a bistable triggering circuit that can detect single photons with extremely high gain [4]. In addition, the SPAD is controlled with a passive quenching circuit which allows for high quantum efficiency and extremely low noise. A combination of these factors and the lack of single-photon background events makes our method ideally suited to characterisation of low average and peak power pulses.

Fig. 1 shows the experimental setup we have used to demonstrate the silicon APD autocorrelator. A 1.555 μm modelocked fibre laser with a 10 GHz repetition rate (Pritel, UOC-1) is used in our demonstration. The laser pulse is launched into a standard Michelson-type autocorrelator and the output of the autocorrelator is focused by a 10X/0.26NA objective lens (Melles Griot). The spot size on the APD is estimated to be $\sim 10 \mu\text{m}$ ($1/e^2$ diameter). The detector is a single photon counting silicon APD module (EG&G, SPCM-AQ-16) with a 160 μm -diameter active region. Two-photon absorption generated photon counts were recorded as a function of the autocorrelator time delay to form the autocorrelation trace.

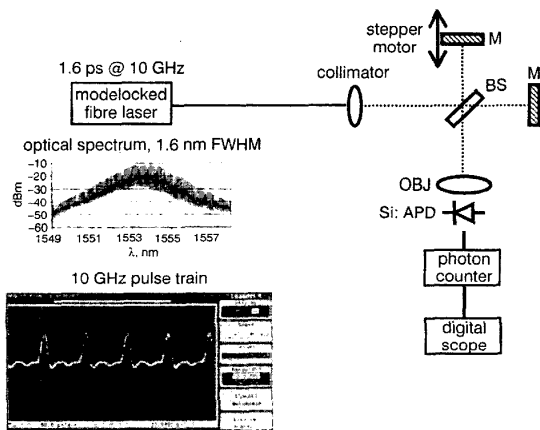


Fig. 1 Autocorrelator schematic diagram

Inset: Modelocked optical spectrum showing 10 GHz fringes and digital scope trace of pulses

Fig. 2 shows the autocorrelation trace obtained with only 7.2 μW of average power incident onto the APD. The full width half maximum (FWHM) of the autocorrelation width is 2.82 ps. If we assume a transform-limited $\text{sec } h^2$ pulse shape, the corresponding 1.67 ps pulsewidth is consistent with the measured 1.6 nm spectral width shown in Fig. 1. Note that high signal-to-noise ratio trace was obtained with a remarkably low average and peak power without the use of a lock-in amplifier. Perhaps more important is the unprecedented low peak power, i.e. 220 μW . Fluctuation in the background could be diminished by increasing the sampling time (currently 1 real sec ~ 0.2 ps of delay). For example, the sampling time can be increased by about a factor of 20 if one does not need to resolve the interference fringes.

We have also measured two-photon generated photon-counts as a function incident power using a singlemode 1575 nm continuous-wave (CW) laser as the excitation source. Comparing with pulsed excitation, a singlemode CW laser provides the advantages that pulsewidth, and more importantly, the exact pulse shape will not affect the measurement. Fig. 3 shows the power dependence curve by varying the incidence power over about two decades. At the lowest power of our measurement, i.e. power levels between 10 and 20 μW , the slope in the log-log plot is about 1.4, indicating some one-photon contribution (possibly due to material defects or band tail). The slope increases to > 1.95 at power levels above 100 μW , indicating negligible one-photon

contribution. Because the ratio of two- and one-photon excitation is proportional to the peak power, our CW excitation results showed that peak power as low as 100 μW is sufficient to be in the two-photon absorption dominated region.

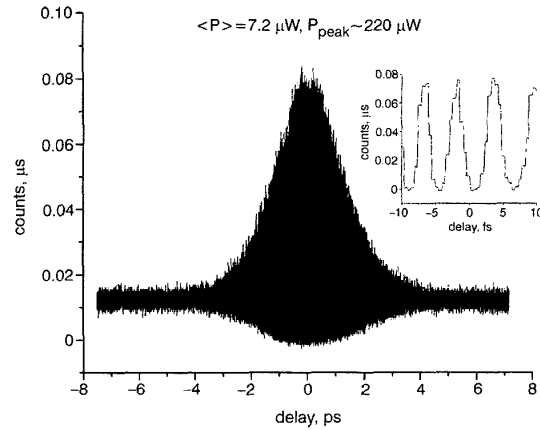


Fig. 2 Interferometric autocorrelation trace yielding 1.67 ps pulse FWHM

Inset: Interference fringes at zero time delay
Data taken with 7.2 μW of average power and 220 μW peak power, yielding a peak power, average power product of $1.5 \times 10^{-3} (\text{mW})^2$

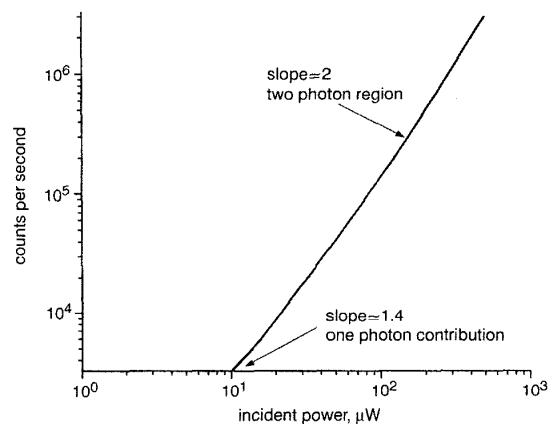


Fig. 3 TPA response of single photon counting silicon APD from singlemode CW laser

The ultra-high sensitivity in measuring two-photon absorption, i.e. the extremely low average and peak power requirement, is provided by the combination of large internal gain of the silicon APD and the photon-counting detection scheme. The large measured TPA response of silicon also agrees with our predicted calculations and those mentioned in the literature [5, 6], and this adds to the two-photon sensitivity. The results could be even further enhanced by focusing to a smaller spot size on the APD, and we estimate another reduction by 10 in the sensitivity figure of merit. Background-free autocorrelations would also be possible with this technique using double-chopping. Other devices with large gain (such as photomultiplier tubes) can also be explored in similar applications, however it may be difficult to exceed the overall performance (sensitivity, compactness, robustness) of the single photon counting silicon APD.

Conclusion: We have shown that direct two-photon absorption in a single photon counting silicon APD provides unprecedented sensitivity in nonlinear autocorrelation measurements, even without the use of lock-in detection. High signal-to-noise ratio trace was obtained at average and peak power product of $1.5 \times 10^{-3} (\text{mW})^2$. One-photon absorption is negligible for peak power levels as low as 100 μW . Such a high sensitivity makes this technique ideally suited in characterising pulses with low average and peak power.

Acknowledgment: The authors acknowledge M.J. Matthews for providing the APD.

© IEE 2002

Electronics Letters Online No: 20020034

DOI: 10.1049/el:20020034

C. Xu (Bell Laboratories, Lucent Technologies, Holmdel, NJ 07733, USA)

J.M. Roth and K. Bergman (Princeton University, Department of Electrical Engineering, Princeton, NJ 08544, USA)

W.H. Knox (The Institute of Optics, University of Rochester, Rochester, NY 14627, USA)

References

- 1 BARRY, L.P., *et al.*: 'Autocorrelation and ultrafast optical thresholding at 1.5 μm using a commercial InGaAsP 1.3 μm laser diode', *Electron. Lett.*, 1998, **34**, (4), pp. 358–360
- 2 LAUGHTON, FR., *et al.*: 'The two-photon absorption semiconductor waveguide autocorrelation', *IEEE J. Quantum Electron.*, 1994, **30**, (3), pp. 838–845
- 3 KIKUCHI, K.: 'Highly sensitive interferometric autocorrelator using Si avalanche photodiode as two-photon absorber', *Electron. Lett.*, 1998, **34**, (1), pp. 123–125
- 4 LI, L., and DAVIS, L.M.: 'Single photon avalanche diode for single molecule detection', *Rev. Sci. Instrum.*, 1993, **64**, (6), pp. 1524–1529
- 5 REID, D.T., *et al.*: 'Commercial semiconductor devices for two photon absorption autocorrelation of ultrashort light pulses', *Appl. Opt. Eng. Lab. Notes*, 1997, **37**, (34), pp. 8142–8144
- 6 XU, C., and DENK, W.: 'Comparison of one- and two-photon optical beam-induced current imaging', *J. Appl. Phys.*, 1999, **86**, pp. 2226–2231

On reduced complexity equalisation for EDGE

N.H. Chow, T.G. Jeans and R. Tafazolli

A reduced complexity equaliser involving the novel reduced-state sequence estimation is presented. It is difficult to employ maximum likelihood sequence estimation for EDGE since it uses the 8PSK modulation scheme and hence high computation complexity is incurred. Consequently, a sub-optimum technique offering an approximation to the optimum performance is required. The proposed method is capable of equalisation with four states, at the expense of only 1 dB trade-off in performance.

Introduction: It was shown in the literature [1, 2] that eight-state delayed-decision feedback sequence estimation (DDFSE) is sufficient for equalisation in EDGE. With reduced-state sequence estimation (RSSE) the complexity can be further reduced through set-partitioning. In this Letter we study the use of RSSE to further reduce the number of trellis states.

Receiver concept: The proposed receiver, shown in Fig. 1, is similar to [2] except for an additional pre-filter block. The fractionally spaced whitened matched filter (WMF), matched to the known transmit pulse is shown to provide sufficient statistics [2, 3]. In EDGE, the training sequence, located at the burst centre, provides a known initial state for the RSSE and therefore requires bi-directional equalisation starting from the centre to the start and end of the burst. A pre-filter is required to transform the overall channel impulse response (OCIR) into its maximum phase equivalent to suit backward equalisation. The pre-filter can be viewed as a WMF but matched to the estimated OCIR. The OCIR refers to the convolution of the transmit filter, channel and WMF. The pre-filter coefficients can be computed using the methods in [4]. Without set-partitioning, the proposed scheme is equivalent to DDFSE [5] and has complexity of 8^μ , where $0 \leq \mu \leq L/2$, L is the length of the $T/2$ -spaced transformed overall channel impulse response (TOCIR), that is the convolution of OCIR and the pre-filter and T is the symbol period. The effect of the remaining TOCIR length is taken into account on a per survivor basis.

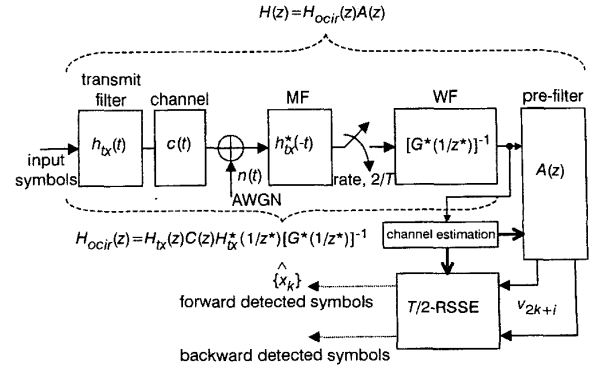


Fig. 1 Complex baseband model

$H_{tx}(z)H_{tx}^*(1/z^*) = G(z)G^*(1/z^*)$; $H_{ocir}(z)H_{ocir}^*(1/z^*) = F(z)F^*(1/z^*)$ and $A(z) = H_{ocir}^*(1/z^*)[F(z)]^{-1}$ and $H_{ocir}^*(1/z^*)[F^*(1/z^*)]^{-1}$ * denote complex conjugate

System model: All signals are represented by their complex baseband equivalents. At the transmitter, random binary data are mapped onto eight PSK symbols as specified in [6]. Equalisation in both directions is identical and only the derivation for forward path is shown although the simulation employs both. The k th received symbol is sampled at rate $2/T$ and the output of the finite-length pre-filter is

$$v_{2k+i} = \sum_{n=0}^{\mu} h_{2n+i}x_{k-n} + v_{2(k-\mu-1)+i} + \eta_{2k+i} \quad i = 0, 1 \quad (1)$$

$$v_{2k+i}^+ = \sum_{n=0}^{L/2-\mu-1-i} h_{2(n+\mu+1)+i}x_{k-n} \quad i = 0, 1 \quad (2)$$

The symbol is $x_k \in \{e^{j2\pi m/8}\}$, $m \in \{0, 1, \dots, 7\}$, $\{h_{2n+i}|i=0, 1\}$, which are coefficients of the TOCIR. $\{v_{2k+i}^+|i=0, 1\}$ represent the effects of the remaining TOCIR which are accounted for by the RSSE using decision feedback in the path metric calculation [5]. The channel is assumed to be constant within each time slot but variable from slot to slot. This model corresponds to low and moderate mobile speeds. Assuming that noise correlation caused by matched filtering is sufficiently removed by the finite-length WMF and remains essentially white after pre-filtering, the noise at its output, $\{\eta_{2k+i}|i=0, 1\}$ is represented as complex, additive white Gaussian noise (AWGN) with zero mean and variance $\sigma_\eta^2 = N_0(W/\text{Hz})$. N_0 is the single-sided power spectral density. The received symbol energy is given by $E_s = \sigma_s^2 \sum_{i=0}^L |h_i|^2 N_s$, the received energy per bit is $E_b = E_s/3$, $\sigma_s^2 = E[|x_k|^2] = 1$ and N_s is the number of samples per symbol. $E[\cdot]$ denote the statistical expectation.

Owing to $T/2$ -spaced operation, the RSSE branch metric Γ_k [2] is modified:

$$\Gamma_k(t_k^{\mu} \rightarrow t_{k+1}^{\mu}) = - \left| v_{2k} - h_{0}x_k(t_k^{\mu} \rightarrow t_{k+1}^{\mu}) - \sum_{l=1}^{\mu} h_{2l}x_{k-l}(t_k) - v_{2(k-\mu-1)}^+ \right|^2 - \left| v_{2k+1} - h_{1}x_k(t_k^{\mu} \rightarrow t_{k+1}^{\mu}) - \sum_{l=1}^{\mu} h_{2l+1}x_{k-l}(t_k) - v_{2(k-\mu-1)+1}^+ \right|^2 \quad (3)$$

$t_k^{\mu} \rightarrow t_{k+1}^{\mu}$ represents the subset transition at epoch k .

Simulation results: The simulation assumes perfect synchronisation and channel estimation. The received pulse is obtained by summing the delayed and sampled version of the shaped pulses corresponding to each ray. The received pulse, the finite-length WMF and pre-filter convolve to form the TOCIR. The channel is assumed to be static, but random. The variance of each ray is defined in the chosen GSM channel models [7].

With eight-state RSSE, performance is similar to that reported in [2], except that its performance for EQ is better. This is because pre-filtering is involved unlike [2] which assumes only forward equalisation without pre-filtering. At low E_b/N_0 , a slight degradation of less than 1.0 and 3.8 dB is observed for four-RSSE and two-state RSSE, respectively at 10^{-1} owing to error propagation.